Pis'ma v ZhETF, vol. 99, iss. 11, pp. 724 – 728

Mapping electromagnetic fields near a subwavelength hole

D. V. Permyakov[+1)], *I. S. Mukhin*[+*], *I. I. Shishkin*[+], *A. K. Samusev*[+], *P. A. Belov*[+], *Yu. S. Kivshar*[+×]

[+]*ITMO University, 197101 St. Petersburg, Russia*

[*]*St. Petersburg Academic University of the RAS, 194021 St. Petersburg, Russia*

[×]*Nonlinear Physics Center, Research School of Physics and Engineering, Australian National University, ACT 0200 Canberra, Australia*

Submitted 27 March 2014
Resubmitted 5 May 2014

We study, both experimentally and theoretically, the scattering of electromagnetic waves by a subwavelength hole fabricated in a thin metallic film. We employ the scanning near-field optical microscopy in order to reconstruct experimentally the full three-dimensional structure of the electromagnetic fields in the vicinity of the hole. We observe an interference of all excited waves with an incident laser beam which allows us to gain the information about the wave phases. Along with the well-known surface plasmon polaritons propagating primarily in the direction of the incident beam polarization, we observe the free-space radiation diffracted by the hole. We compare the experimental results with the fields of pure electric and pure magnetic dipoles as well as with direct numerical simulations. We confirm that a single hole in a thin metallic film excited at the normal incidence manifests itself as an effective magnetic dipole in the visible spectral range.

DOI: 10.7868/S0370274X14110034

Introduction. The use of nanophotonics for guiding light is of a great importance for numerous potential applications of optical structures operating at the subwavelength scale. The development of nanophotonics is closely linked to material science being able to fabricate the structures at the nanoscale for the subwavelength guiding of light. One of the major research directions in nanophotonics is associated with the use of metals which allow guiding collective excitations of the electromagnetic fields and electrons in the form of surface plasmon polaritons (SPPs) localized in the vicinity of metal-dielectric interfaces [1–5]. The simplest structure allowing to excite SPPs is a single hole in a thin metallic film, that generates SPPs after probing the film by an electromagnetic plane wave [6, 7].

On the other hand, an important tool in the modern nanophotonics is the scanning near-field optical microscope (SNOM) which allows to obtain the information about the structure of electromagnetic fields in the vicinity of nanoscale objects with the subwavelength resolution [8–10]. In the aperture-based SNOM devices, a key role is played by a metallized tip with an aperture diameter of the order of 100 nm. A number of theoretical and experimental papers has been devoted to the study of light emerging from the subwavelength holes [11–16] and the properties of light collected by a SNOM fiber tip [17–19]. A special attention has been paid to the studies of the SPP-supported transmission of a single hole and hole arrays [15, 20–23]. Nevertheless, to the best of our knowledge, there exists no full experimental studies of the structure of the electromagnetic field energy distribution near a single subwavelength hole fabricated in a metallic thin film.

Very recently, N. Rotenberg et al. [24, 25] used polarization-resolved near-field measurements to separate and quantify the electric and magnetic optical response of subwavelength holes in a thick gold film. Their study provided experimental access and theoretical understanding of the electromagnetic polarizability that describes the optical response of metallic holes, but the complete picture of the electromagnetic fields near subwavelength holes made in thin metallic films is still missing.

In this Letter, we apply the SNOM technique and perform the complete experimental three-dimensional reconstruction of the electromagnetic fields in the vicinity of a subwavelength hole fabricated in a thin metallic film. We confirm experimentally and also by employing extensive numerical simulations, as well as through a comparison with the field structures generated by pure electric and pure magnetic dipole sources, that a single subwavelength hole in a metallic film excited by an

[1)]e-mail: d.permyakov@phoi.ifmo.ru

electromagnetic wave at the normal incidence behalves primarily as an effective magnetic dipole in the visible spectral range.

Experimental samples and setup. We study the transmission of light through a subwavelength hole drilled with focused ion beam (FIB) in 75-nm-thick silver film deposited on a glass substrate. The sample structure and scanning electron micrograph of sample's surface are depicted in Fig. 1. Since the roughness of

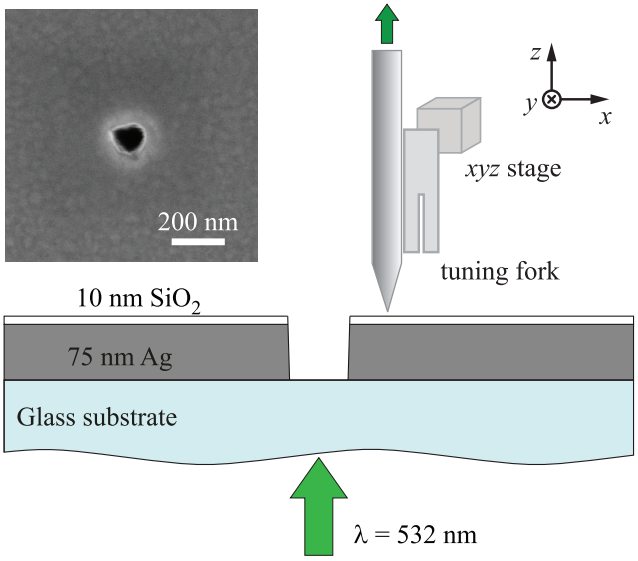

Fig. 1. Experimental setup and sample structure (a detailed description is given in the text). The inset in the top-left corner is a SEM micrograph of the subwavelength hole with the diameter ≈ 100 nm drilled by means of the FIB technology in a thin silver film

a metal surface affects dramatically the propagation length of SPPs, we examine a set of samples which represent a silver film on a glass substrate obtained by means of thermal evaporation with different deposition rates. The best surface roughness with rms = 2.2 is achieved with the rate of 2 nm per second. The sample is also covered with a 10-nm-thick SiO_2 sputtered with magnetron deposition technique passivating layer in order to protect Ag from oxidation and sulfatation. The thickness of the metallic film is optimized, so that the amplitudes of electromagnetic fields of the excited waves and a probing beam transmitted through the sample would be of the same order. This give us a possibility to observe the interference between these waves and to gain useful information about the phases of all excited waves.

In our experiments, we employ the aperture-type SNOM (AIST-NT CombiScope Scanning Probe Microscope with optical aluminium-coated fiber probe) operating in the collection mode, as shown schematically in Fig. 1. A fiber probe is glued to a tuning fork that is used to control the tip-to-surface distance in the shear-force mode by keeping the magnitude of the tip oscillations on a preselected level. The sample is excited by a green laser ($\lambda = 532$ nm) focused with either achromatic doublet lens ($F = 50$ mm) or by Olympus 20X objective for obtaining different focal spot sizes. An optical signal collected by a probe is measured with a photomultiplier tube (Hamamatsu H10722-01).

Scanning is performed both in contact and plane scan modes. Such a regime allows us to perform the scanning within a plane relying on the sample surface with the preselected lift value. The latter mode is employed to perform scanning within a set of planes on different elevations and to perform the three-dimensional reconstruction of the field energy density, as discussed below.

Surface plasmon polaritons. The SNOM image obtained at the elevation of 200 nm over the sample surface is presented in Fig. 2a. The laser beam is focused on the subwavelength hole with a long-focal lens. Along with the Gaussian background originated from the transmitted probing laser beam, we observe an interference pattern with the radial and angular dependencies of the oscillation amplitude. These oscillations have the maximal amplitude along the horizontal sec-

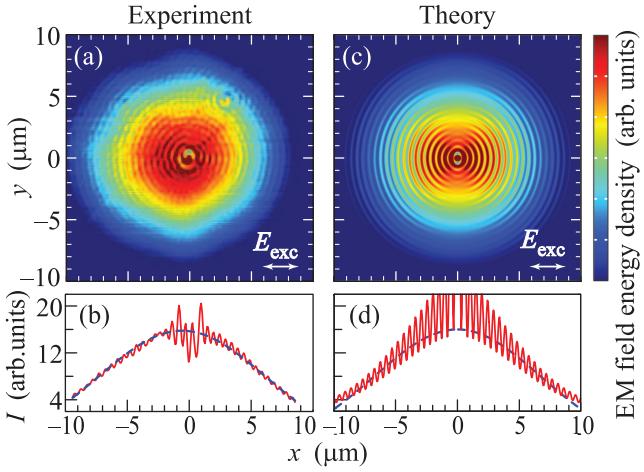

Fig. 2. Comparison between the experimental and numerical results. (a) – SNOM image obtained from the hole in a silver film at the elevation of 200 nm above the sample surface. Polarization of the incident beam is parallel to the x-axis. (b) – Horizontal cross-section of the image in Fig. a made through the center of the hole. (c), (d) – Numerically calculated energy density of the electromagnetic field and its cross-section in the geometry corresponding to Figs. a, b, respectively

tion of the image that goes through the center of the hole, i.e. along the direction of polarization of the incident beam. The measured intensity profile along this section is shown in Fig. 2b.

In order to verify our experimental results, we perform numerical simulations in CST Microwave Studio® package. The distribution of electromagnetic field energy density is shown in Fig. 2c and d. It is important to justify here two assumptions. First, it is worth mentioning that it is permissible to neglect the influence of the probe on the excitation of the nanohole within the whole $20 \times 20\,\mu\text{m}^2$ large scanning area except its very center. Second, according to the results of the numerical simulations, all the features of the interferometric phenomena discussed in this section are observed in both electric and magnetic fields. Therefore, for the sake of simplicity we compare the experimental data to the electromagnetic field energy density in Fig. 2 instead of unnecessary applying more complicated models [17, 19].

The measured period of oscillations is $\approx 500\,\text{nm}$, which is less than the wavelength of exciting radiation $\lambda = 532\,\text{nm}$ and therefore this interference is not likely concerned with scattered free-space wave modes. At the same time, one can expect to observe SPPs on the silver/air interface [6, 26] with the wavelength

$$\lambda_{\text{SPP}} = \lambda \left(\frac{\text{Re}(\varepsilon_m) + 1}{\text{Re}(\varepsilon_m)} \right)^{1/2} \approx 508\,\text{nm}, \qquad (1)$$

taking into account the value of permittivity of Ag, $\varepsilon_{\text{Ag}} \approx -11.7 + 0.4i$ [27].

Such SPPs are the propagating TM-polarized modes localized in the vicinity of the metal surface with the wavevector $\mathbf{k}_{\text{SPP}}$ and possessing two non-zero Cartesian components of the electric field. One of the electric field components is directed along $\mathbf{k}_{\text{SPP}}$, and the other one is perpendicular to the metal-dielectric interface. The linearly polarized incident beam has only E_x non-zero component of the electric field in its focal plane, therefore the angular dependence of the interference pattern can be easily understood: it is absent in the y-direction and it has the maximal amplitude along the x-axis. In general, the interferometric term is proportional to $\cos\phi$, where ϕ is the azimuthal angle of the observation point in the xy-plane.

Experimental and numerical data presented in Fig. 2 demonstrate qualitative agreement, but there are some quantitative differences. The first one is the amplitude of intensity modulation in the simulations and experiment (see Figs. 2c and d). This can be concerned with imperfections in the shape of hole edges that affect the efficiency of the SPP excitation. The second difference is observed between the measured period of oscillations and the theoretically calculated SPP wavelength, that can be caused by an imperfect focusing of a laser beam which leads to inhomogeneity of the incident beam phase along the beam section.

In order to prove that the oscillations discussed above correspond to SPPs and to obtain the full picture of the interaction of light with a subwavelength hole made in a thin metallic film, we perform 37 scans with different elevations above the sample surface from 5 nm up to 5 μm. After the interpolation of the data, we obtain the three-dimensional distribution of the electromagnetic fields summarized in Fig. 3a. We observe that

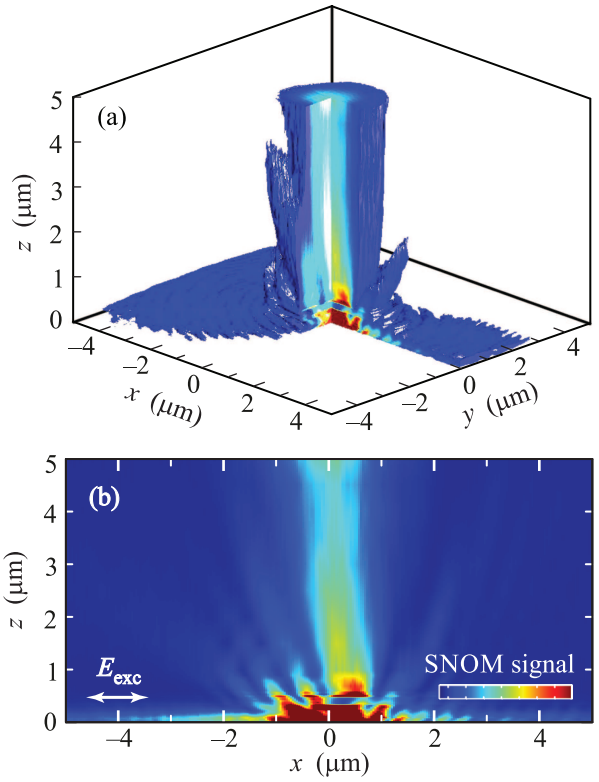

Fig. 3. (a) – Experimentally reconstructed three-dimensional structure of the electromagnetic fields plotted as an isosurface at 40 % level of the maximum value. (b) – xz-section of the reconstructed field distribution

the wave involved in the interference with an incident beam shown in Figs. 2a and b is localized in the vicinity of the sample surface. This gives us the further strong support to the fact that this wave is the SPP excited by the hole.

Subwavelength hole as a magnetic dipole. Along with the features concerned with SPPs, the xz-section of the SNOM signal observed in the experiment (see Fig. 3b) contains additional interferometric pattern over the sample surface. These maxima are a conse-

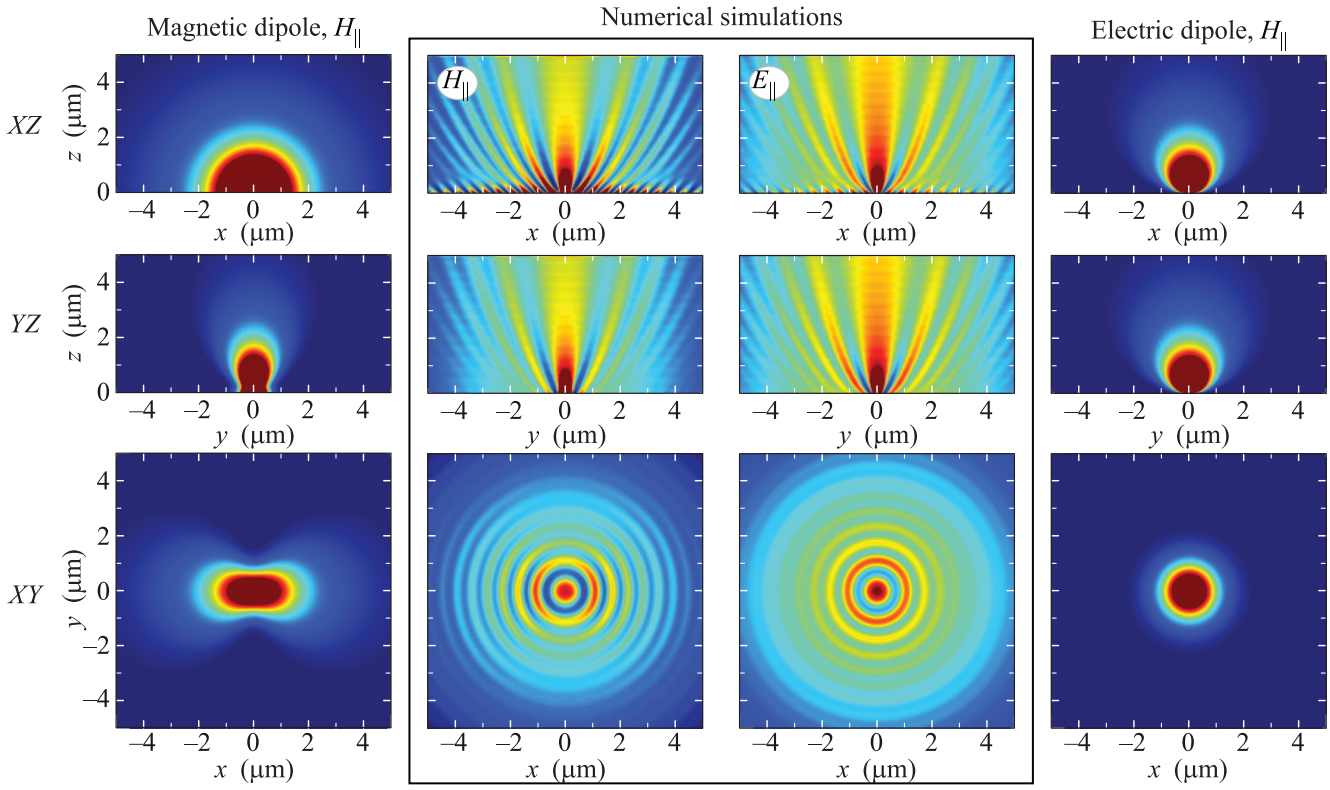

Fig. 4. Numerical xz, yz and xy cross-sections of the three-dimensional electromagnetic fields for different cases. Two central columns: numerically simulated energy densities of the lateral magnetic ($|H_x|^2 + |H_y|^2$) and electric ($|E_x|^2 + |E_y|^2$) fields near a subwavelength hole. The bottom row shows the images obtained at the distance of $z = 1\,\mu$m from the sample. Left and right columns show the lateral magnetic energy density for the pure electric and magnetic dipoles, respectively

quence of the waves emerged from the hole into the free space interfering with the probing beam. To analyze the nature of this radiation, we neglect low radiating high-order multipole moments and assume, in the first approximation, that the nanohole is a point-like dipole source of free- space waves.

In order to understand how the near-field probe collects the far-fields of the electric (ED) and magnetic (MD) dipoles, we resort to a theoretical model based on the reciprocity theorem approach [17] that has been recently verified experimentally [19] for the case of near fields measured in the vicinity of a photonic crystal waveguide. According to this approach, the near-field aperture probe is sensitive only to the lateral components of the electromagnetic fields. In the case of far-field radiation, this model leads to a conclusion that the near-field probe acts as a "magnetic analyzer" collecting mainly lateral magnetic fields [18, 28]. Below, we consider far-field radiation of a single nanohole collected by a near-field aperture probe, therefore, further discussion will be held in the term of the lateral magnetic field energy density $|H_x|^2 + |H_y|^2$.

Figs. 4, left and right, show the lateral magnetic energy maps for MD and ED [29]. It is important to emphasize that contrary to the case of MD in Fig. 4, left, these fields posses rotational symmetry along z-axis for the ED in Fig. 4, right. Further on, we notice that the electric and magnetic fields of ED and MD with their respective dipole moments $\mathbf{p}$ and $\mathbf{m}$ are complimentary: for the ED one can make substitutions $\mathbf{p} \to \mathbf{m}$, $\mathbf{E} \to \mathbf{H}$, and $\mathbf{H} \to -\mathbf{E}$ in order to obtain correct expressions for the fields of MD [29]. Therefore, we come to the conclusion that both lateral magnetic fields for ED and lateral electric fields for MD possess cylindrical symmetry, whereas magnetic fields of MD and electric fields for ED do not.

Fig. 4, middle shows numerically calculated energy densities of the lateral magnetic and electric fields in the vicinity of the nanohole excited by a Gaussian beam with the beam waist $w_0 = 19\,\mu$m. The xy sections at the bottom of Fig. 4 are taken at the elevation of $z = 1\,\mu$m to observe the field patterns of free-space waves with negligible contribution of the SPP. The xy section in Fig. 4, middle shows strong azimuthal dependence of

the pattern of the lateral magnetic fields. This leads directly to the conclusion that the nanohole possesses strong MD dipole response as long as these fields of ED are cylindrically symmetric (Fig. 4, right). On the other hand, the lateral electric fields in xy section Fig. 4, middle demonstrate no vivid dependence on the azimuthal angle, which allows us to conclude that the magnitude of ED contribution to the fields radiated by the nanohole is weak. Thus, a subwavelength hole in metallic film excited by a wave normal to the surface acts as a pure MD in the visible spectral range.

Concluding remarks. We have reconstructed, both experimentally and numerically, the full three-dimensional structure of the electromagnetic fields generated due to the interaction of a laser beam with a subwavelength hole in a thin metallic film. We have made a direct comparison of the obtained experimental data with the results of numerical simulations. A small thickness of the metallic film allowed us to observe the interference of the incident beam transmitted through the hole with all of the waves excited by the hole, gaining an important information about the phases of all waves. We have demonstrated that a hole in a metallic film acts as a point-like source of SPPs propagating primarily in the direction of the electric field of the probing laser beam. At the same time, the three-dimensional reconstruction of the electromagnetic fields allows us to investigate the structure of the light transmitted through the subwavelength hole. Our results confirm that a subwavelength hole in a metallic film excited by an electromagnetic wave at the normal incidence manifests itself as a pure point-like magnetic dipole source in the visible spectral range.

We are grateful to D.A. Kudryashov for assistance in the sample preparation. This work was supported by the Government of the Russian Federation (grant # 074-U01), the Ministry of Education and Science of the Russian Federation (project # 11.G34.31.0020), the Russian Foundation for Basic Research (project # 14-02-31765), and the Australian National University.

1. W. L. Barnes, A. Dereux, and T. W. Ebbesen, Nature **424**, 824 (2003).
2. S. I. Bozhevolnyi, V. S. Volkov, E. Devaux, J. Y. Laluet, and T. W. Ebbesen, Nature **440**, 508 (2006).
3. X. Li, L. Huang, Q. Tan, B. Bai, and G. Jin, Opt. Express **19**, 6541 (2011).
4. J. Zhang, L. Zhang, and W. Xu, J. Phys. D: Appl. Phys. **45**, 113001 (2012).
5. B. B. Tsema, Y. B. Tsema, M. R. Shcherbakov, Y.-H. Lin, D.-R. Liu, V. V. Klimov, A. A. Fedyanin, and D. P. Tsai, Opt. Express **20**, 10538 (2012).
6. L. Yin, V. K. Vlasko-Vlasov, A. Rydh, J. Pearson, U. Welp, S. H. Chang, S. K. Gray, G. C. Schatz, D. B. Brown, and C. W. Kimball, Appl. Phys. Lett. **85**, 467 (2004).
7. S. H. Chang, S. Gray, and G. Schatz, Opt. Express **13**, 3150 (2005).
8. D. W. Pohl, W. Denk, and M. Lanz, Appl. Phys. Lett. **44**, 651 (1984).
9. B. Hecht, B. Sick, U. P. Wild, V. Deckert, R. Zenobi, O. J. F. Martin, and D. W. Pohl, J. Chem. Phys. **112**, 7761 (2000).
10. L. Novotny and B. Hecht, *Principles of Nano-optics*, Cambridge University Press (2012).
11. H. A. Bethe, Phys. Rev. **66**, 163 (1944).
12. C. Bouwkamp, Philips Res. Rep. **5**, 401 (1950).
13. V. Klimov and V. Letokhov, Opt. Commun. **106**, 151 (1994).
14. R. Wannemacher, Opt. Commun. **195**, 107 (2001).
15. C. Genet and T. W. Ebbesen, Nature **445**, 39 (2007).
16. I. V. Treshin, V. V. Klimov, P. N. Melentiev, and V. I. Balykin, Phys. Rev. A **88**, 023832 (2013).
17. J. A. Porto, R. Carminati, and J. J. Greffet, J. Appl. Phys. **88**, 4845 (2000).
18. H. Kihm, S. Koo, Q. Kim, K. Bao, J. Kihm, W. Bak, S. Eah, C. Lienau, H. Kim, P. Nordlander, N. Halas, N. Park, and D. S. Kim, Nat. Commun. **2**, 451 (2011).
19. B. le Feber, N. Rotenberg, D. M. Beggs, and L. Kuipers, Nat. Photonics **8**, 43 (2014).
20. T. Ebbesen, H. Lezec, H. Ghaemi, T. Thio, and P. Wolff, Nature **391**, 667 (1998).
21. F. J. García de Abajo, J. J. Sáenz, I. Campillo, and J. S. Dolado, Opt. Express **14**, 7 (2006).
22. D. N. Neshev, A. Minovich, T. Dieing, H. T. Hattori, I. McKerracher, H. H. Tan, C. Jagadish, and Yu. S. Kivshar, Phys. Status Solidi: Rapid Reserach Letters **4**, 253 (2010).
23. F. J. Garca-Vidal, L. Martin-Moreno, T. W. Ebbesen, and L. Kuipers, Rev. Mod. Phys. **82**, 729 (2010).
24. N. Rotenberg, M. Spasenović, T. L. Krijger, B. le Feber, F. J. García de Abajo, and L. Kuipers, Phys. Rev. Lett. **108**, 127402 (2012).
25. N. Rotenberg, T. L. Krijger, B. le Feber, M. Spasenović, F. J. García de Abajo, and L. Kuipers, Phys. Rev. B **88**, 241408(R) (2013).
26. L. Yin, V. K. Vlasko-Vlasov, J. Pearson, J. M. Hiller, J. Hua, U. Welp, D. E. Brown, and C. W. Kimball, Nano Lett. **5**, 1399 (2005).
27. P. B. Johnson and R. W. Christy, Phys. Rev. B **6**, 4370 (1972).
28. H. W. Kihm, J. Kim, S. Koo, J. Ahn, K. Ahn, K. Lee, N. Park, and D. S. Kim, Opt. Express **21**, 5625 (2013).
29. J. D. Jackson, *Classical Electrodynamics*, 3rd Ed., Wiley-VCH (1998).